Clustering of microscopic particles in constricted blood flow

Christian Bächer, Lukas Schrack, and Stephan Gekle
Biofluid Simulation and Modeling, University of Bayreuth, Universitätsstraße 30, 95440 Bayreuth, Germany
(Received 23 August 2016; published 23 January 2017)

A mixed suspension of red blood cells (RBCs) and microparticles flows through a cylindrical channel with a constriction mimicking a stenosed blood vessel. Our three-dimensional Lattice-Boltzmann simulations show that the RBCs are depleted right ahead of and after the constriction. Although the RBC mean concentration (hematocrit) is 16.5% or 23.7%, their axial concentration profile is very similar to that of isolated tracer particles flowing along the central axis. Most importantly, however, we find that the stiff microparticles exhibit the opposite behavior. Arriving on a marginated position near the channel wall, they can pass through the constriction only if they find a suitable gap to dip into the dense plug of RBCs occupying the channel center. This leads to a prolonged dwell time and, as a consequence, to a pronounced increase in microparticle concentration right in front of the constriction. For biochemically active particles such as drug delivery agents or activated platelets this clustering may have important physiological consequences, e.g., for the formation of microthrombi.

DOI: 10.1103/PhysRevFluids.2.013102

I. INTRODUCTION

Blood mostly consists of highly deformable red blood cells (RBCs) occupying from 15 up to 45 volume percent [1–4]. When flowing through a channel or blood vessel, RBCs preferentially travel in the low-shear zone around the channel center. Stiff particles such as white blood cells, platelets or synthetic microparticles are thereby forced to flow near the channel walls. This well-known effect, called margination, is of physiological relevance, e.g., for platelets where a near-wall position allows them to quickly stop bleeding in case of vessel injury. For synthetic particles such as drug delivery agents a near-wall position is essential to directly deliver their cargo to endothelial cells, thus minimizing unwanted distribution of pharmaceutical agents through the vascular system.

In 1980 margination was first observed experimentally [5]. Since then, a large number of studies have investigated the phenomenon by means of experiments [6–15] or simulations [13,16–37]. All these works focus on spatially constant geometries like straight pipes, rectangular channels, or plane-Couette systems. However, more complex geometries such as bifurcations or constrictions (stenoses) are a common feature of the vascular system. At the same time, investigations of marginated particles near such geometrical features are scarce. For RBCs a recent detailed study in cylindrical microchannels with stenosis exists [38]. Reference [39] presented two-dimensional (2D) simulations near aneurysms, Ref. [40] investigated the recirculation zones after a sudden expansion and Refs. [41,42] focused on the displacement of RBCs when flowing through a constricted microchannel. Near a stenosis Ref. [43] presented local velocity fields, while other studies treated the dynamics of platelets in 2D and plane-Couette geometries [44,45].

Here we use three-dimensional (3D) Lattice-Boltzmann simulations to study margination of stiff spherical and ellipsoidal microparticles in an RBC suspension flowing through a cylindrical channel with a constriction mimicking the geometry of a stenosed blood vessel. While the radial concentration profile is found to be qualitatively unaffected (RBCs in the center, microparticles near the wall) we find that the concentration profile along the axial direction varies significantly for both RBCs and microparticles. Right in front of the constriction we observe a decrease in RBC concentration which can be almost quantitatively explained by the flow acceleration using passive point particles flowing along the central axis as the most simple model system. Microparticles, on the other hand, exhibit the opposite behavior: their concentration in front of the constriction increases significantly. This effect

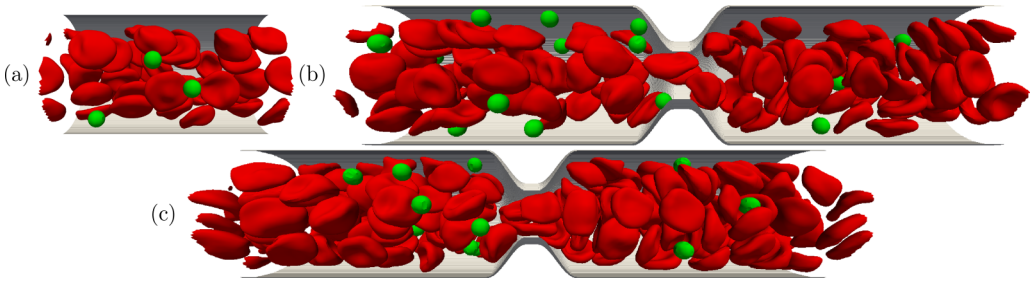

FIG. 1. Snapshot of the simulated system. (a) Straight cylindrical channel with 47 RBCs and four microparticles (Ht = 16.5%). (b) Constricted channel with 108 RBCs and 18 microparticles (Ht = 16.5%) and (c) with 151 RBCs and 18 microparticles (Ht = 23.7%). The ratio between the radii of the constricted and the straight cylinder is 1/2. A periodic boundary condition in flow direction is used. The flow is from left to right.

can be traced back to the near-wall trajectories on which microparticles travel in the straight channel section before arriving at the constriction and seems to be strongly reinforced by the cylindrical geometry since a recent study in planar geometries [45] did not report it. In order to pass through the constriction, the particles need to leave this position and squeeze into the densely packed RBC layer. This lowers the microparticles' passing rate leading to a pronounced peak in microparticle concentration ahead of the constriction.

II. MATERIALS AND METHODS

We perform our simulations by means of a 3D Lattice-Boltzmann method (LBM) implemented in the simulation package ESPResSo [46–48] extended by an immersed boundary method (IBM) algorithm [49,50]. The LBM uses the spatially and temporally discretized Boltzmann equation to calculate fluid behavior [51–53]. The fluid in which the particles are suspended is chosen to mimic blood plasma with a density of $1000\,\mathrm{kg/m^3}$ and a viscosity of $\mu = 1.2 \times 10^{-3}\,\mathrm{Pa\,s}$. The simulation package ESPResSo enables us to add thermal fluctuations with a temperature $T = 300\,\mathrm{K}$ using a multiple-relaxation-time scheme. This scheme contains more free parameters than the common Bhatnagar-Gross-Krook (single relaxation time), which in turn can be used to add thermal fluctuations satisfying the fluctuation-dissipation theorem [48,52]. We note, however, that due to the large size of the RBCs and particles, thermal fluctuations are not expected to have any detectable influence on the effects discussed in this work. The grid size for the main setup shown in Figs. 1(b) and 1(c) is $180 \times 44 \times 44$.

Both RBCs and microparticles are realized via the IBM. The RBC diameter is chosen to be $7.82\,\mu\mathrm{m}$. The RBC membrane is modeled as an infinitely thin elastic sheet which is discretized by a set of nodes that are treated as Lagrangian points flowing with the fluid and that are connected by triangles. The forces exerted by the membrane on the fluid are calculated every time step by interpolating between the fluid nodes using an eight-point stencil. For the elastic properties we use the Skalak model [54–57] with a shear modulus $k_S = 5 \times 10^{-6}\,\mathrm{N/m}$ and an area dilatation modulus $k_A = 100 k_S$. Bending forces are computed via the Helfrich model with a bending modulus $k_B = 2 \times 10^{-19}\,\mathrm{Nm}$ [4,58] using the bending algorithm which is denominated method A in Ref. [58]. In this commonly used approach the bending energy is simply proportional to the angle between two neighboring triangles. The actual forces on the IBM nodes are obtained by differentiating analytically this bending energy with respect to the node positions. We note that, while this rather simplistic algorithm is clearly not the most accurate method, it should be sufficient for the present purpose, where the major focus is on the behavior of the microparticles, not the RBCs themselves. To ensure numerical stability, we use an empirical volume conservation potential [35] as well as a short-ranged soft-sphere repulsion. The latter decays as r^{-4} where r is the distance between two microparticles

or RBCs and is applied only when the distance falls below one LBM grid cell. The same repulsive potential is also applied between microparticles or RBCs and the channel wall. The RBC membrane contains 1280 triangles and 642 nodes such that the average distance between two surface nodes is similar to the spacing of the LBM grid. This criterion also determines the discretization chosen for the different microparticle shapes.

The spherical microparticles have a diameter of $a = 3.2\,\mu$m and are thus in a range for which strong margination was recently reported [29]. Numerically, they follow the same model as the RBCs, but with 1000 times higher shear and bending moduli. In addition, they are stiffened by a 3D lattice inside the particle with lattice constant of one LBM grid cell. The grid is connected to the shell by elastic springs and a bending potential. The stability of our particle model is documented in Ref. [34].

The constriction is modeled by two straight cylinders with different radii and a transition zone between them. To provide a smooth transition the radius in the transition zone follows a third order polynomial such that the function describing the boundary and its first derivative are continuous. To control the flow rate a spatially constant body force mimicking an external pressure gradient is applied. The Reynolds number calculated from the centerline velocity, the RBC radius R_{RBC}, and the kinematic viscosity of the fluid ν is $\mathrm{Re} = \frac{R_{RBC} \cdot v}{\nu} = O(10^{-3})$. The time step is chosen to $0.06\,\mu$s.

At the beginning of the simulation the RBCs and the microparticles are inserted with a regular pattern. The system is then run until all remnants of this regular initial configuration have vanished and a steady state is achieved. Concentration profiles are obtained by time-averaging starting from these random configurations. The systems are simulated for about 10 s.

The axial and radial concentration is calculated by dividing the system into axial and radial bins. At every time step RBCs and microparticles are sorted into corresponding bins using their center-of-mass. The concentration is calculated by dividing the averaged number of particles inside one bin by the volume of the bin.

III. RESULTS AND DISCUSSION

A straight channel as comparison, and two examples of the investigated systems with stenosis are shown in Fig. 1. In all cases the cylinder radius is $R_C = 13.4\,\mu$m, and in Figs. 1(b) and 1(c) the ratio between the radius of the constricted part and the main cylinder is 1/2. The length of the region with constant lower radius here is $2.6\,\mu$m but will be varied below. The length of the straight channel is 47 and $117\,\mu$m for the constricted channel. We verify in the Supplemental Material [59] that varying the channel length has no influence on the results. The hematocrits are 16.5% in Fig. 1(a) and Fig. 1(b) and 23.7% in Fig. 1(c). The mean RBC velocity is $V = 1.7\ \mathrm{mm\,s^{-1}}$ in the main channel in Fig. 1(a) and $V = 1.3$ and $V = 0.8\ \mathrm{mm\,s^{-1}}$ inside the constriction in Fig. 1(b) and Fig. 1(c), respectively. These numbers represent typical values occurring in the microcirculation [1]. The corresponding capillary numbers $\mathrm{Ca} = \mu V / k_s$ are 0.41, 0.31, and 0.19. The wall shear rates (for the full flow including RBCs) were determined by a linear fit to the velocity profile near the wall as $280\ \mathrm{s^{-1}}$, $130\ \mathrm{s^{-1}}$, and $100\ \mathrm{s^{-1}}$, respectively.

A. Center-of-mass distribution in comparison to straight cylinder

We first extract two-dimensional concentration profiles in the x-r plane, where x is the coordinate along the channel and r is the radial position in cylindrical coordinates. Local concentrations of RBCs and microparticles are calculated from their center-of-masses as described in the Methods section. The result for the straight channel is shown in Fig. 2(a) for RBCs and in Fig. 2(b) for microparticles. The RBC concentration is rather homogeneous, and the RBCs are located around the channel center since their deformability causes the RBCs to migrate to the center [60–62]. Near the channel wall, the well-known cell-free layer with almost zero RBC concentration is visible [63–65]. As can be seen in Fig. 2(b) the microparticles are expelled into this cell-free layer leading to a sharply peaked concentration distribution of the marginated microparticles. The origin of

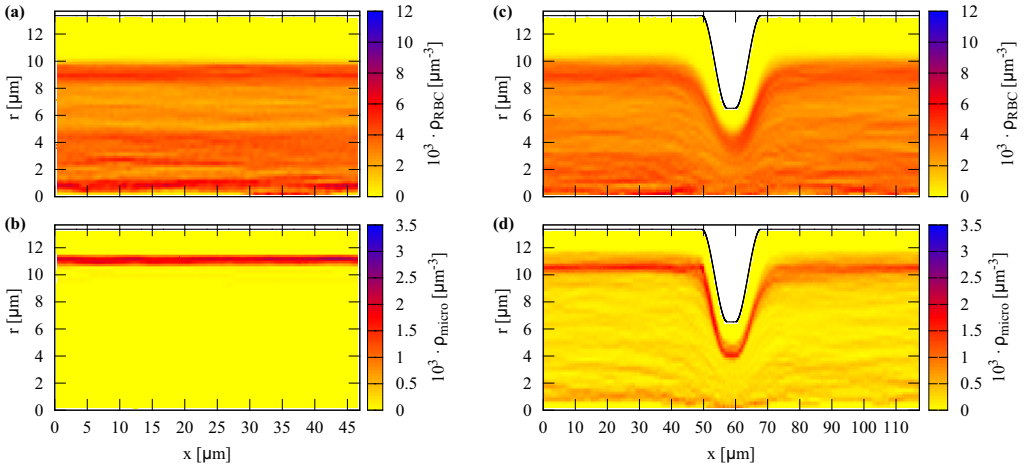

FIG. 2. Concentration as a function of the radial and axial position plotted for the (a) RBCs and (b) microparticles in the straight cylinder and for the (c) RBCs and (d) microparticles in a cylinder with constriction. The channel geometry is illustrated by the black line.

microparticle migration into the cell-free layer is commonly attributed to heterogeneous collisions with the RBCs [18,20,23,27,32,34,37,45].

The general picture looks similar for the constricted channel with Ht = 16.5% as shown in Figs. 2(c) and 2(d) (see Supplemental Material for Ht = 23.7% [59]). Besides a reduced cell-free layer inside the constriction, which agrees well with Ref. [38], the RBC concentration in the channel center is not significantly influenced by the constriction. The peak at large radii in the microparticle concentration is, however, more blurred compared to the straight channel, especially right behind the constriction. This can be explained since the microparticles require a certain time (or, equivalently, distance) in order to regain their fully marginated state after passing through the constriction. Nevertheless, the vast majority of microparticles is in a marginated position even in the constricted channel.

B. Axial distribution in one-component suspensions

In order to assess more quantitatively a possible influence of the constriction, we investigate one-dimensional axial concentration profiles, which correspond to integrating the 2D concentration profiles of Fig. 2 over the radial position. To discriminate between the generic influence of the constriction and the influence of margination we start by considering single-component suspensions where margination is not present. In Fig. 3(a) we show the concentration profile for a pure RBC suspension, which has been created by replacing all microparticles by RBCs in the system of Fig. 1(b). Far from the constriction the concentration exhibits a constant plateau as expected in a straight channel. Upon entering the constriction, the concentration first decreases and then rises again until a roughly constant plateau inside the constriction is reached. At the exit, the concentration decreases a second time and soon thereafter recovers its straight channel level. Removing the RBCs from the system in Fig. 1 and leaving only the 18 microparticles leads to the concentration profile in Fig. 3(b). The microparticle concentration profile looks remarkably similar to that of the pure RBCs pointing to a common generic origin.

In order to explain these observations, we revert to the most simple model system: passive tracer particles flowing along the central axis through the constriction. For this, we first extract the velocity profile from a simulation without any particles and thermal fluctuations [Fig. 3(c) green curve]. We then compute the position as a function of time for a train of tracer particles which precisely follow this velocity. Due to periodic boundary conditions the particles repeatedly pass the

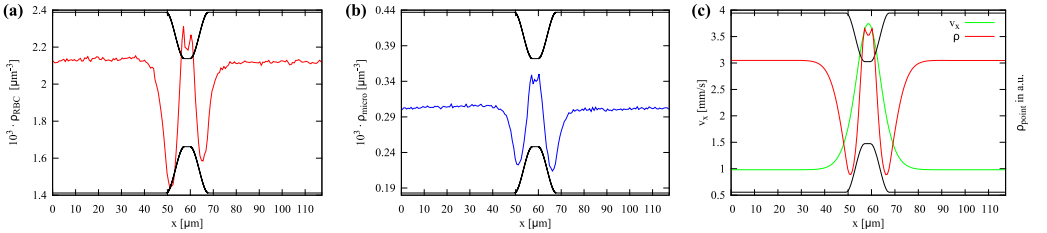

FIG. 3. Concentration as a function of the axial position for a pure RBC suspension (a) and for a pure microparticle suspension (b). Despite very different particle properties and mean concentrations both profiles are remarkably similar. (c) The axial flow velocity on the centerline for the pure liquid without thermal fluctuations (green curve). The concentration distribution for a train of passive tracer particles following this velocity profile (red curve) well reproduces the concentration profiles of the single-component suspensions in (a) and (b). The channel geometry is illustrated by the black line.

constriction allowing us to compute the time-averaged concentration profile, which is shown as the red line in Fig. 3(c). The profile of this simple system looks almost the same as the ones from the more complex RBC and microparticle suspensions. This furnishes a straightforward explanation for the concentration profiles: upon entering the constriction the fluid velocity rises due to mass conservation leading to an acceleration of a flowing particle. The acceleration increases the distance to the following particle and thus causes a concentration decrease. Inside the constriction, this effect, however, is (over-)compensated by the reduced channel radius, leading to a plateau which is slightly higher than the straight channel value. At the exit of the constriction the opposite dynamics is observed. It remains remarkable that the concentration profile of the RBC suspension in Fig. 3(a) and the microparticle suspension in Fig. 3(b) can be well reproduced by passive tracer points. The only exception is that the RBC densities in front of and behind the constriction are slightly asymmetric, while those of the particle train in Fig. 3(c) are perfectly symmetric as expected under Stokes flow conditions. Similar asymmetries in RBC concentration have also been observed by Ref. [38] and (in planar channels) by Ref. [45]. The most likely source for the asymmetry lies in the RBC deformability.

C. Clustering of microparticles at constrictions in mixed suspensions

We now consider the mixed RBC and microparticle suspension with Ht = 16.5% as shown in Fig. 1(b). Due to their position in the channel center the RBCs in this system are not affected by the small number of microparticles and exhibit the same behavior as in the pure RBC system [Fig. 3(a)] as demonstrated by the red curve in Fig. 4(a). In stark contrast, the microparticle concentration shown by the blue line in Fig. 4(a) is completely changed by the presence of the RBCs. Instead of a decrease, the concentration in front of the constriction now exhibits a pronounced increase. At the exit of the constriction the same dip in the concentration appears as seen before for the pure microparticle suspension in Fig. 3(c).

The increase of the microparticle concentration in front of the constriction, which is our main result, can only be explained by the interplay of margination and constriction. Due to their deformability the RBCs migrate to the channel center and are thus able to pass relatively unhindered through the constriction. The dense central plug of RBCs, however, acts as a barrier for the microparticles. Arriving on a marginated position at the channel walls, in order to pass the constriction, they need to penetrate the RBC plug. The collisions with the RBCs counteract this motion, resulting in a longer dwell time in front of the constriction. This causes the peak in the microparticle concentration.

Indeed, this mechanism is demonstrated by the radial concentration profiles in Fig. 4(c) in the region close to the constriction. Before and after the constriction the microparticles are clearly located inside the cell-free layer well separated from the RBCs. Entering the constriction the

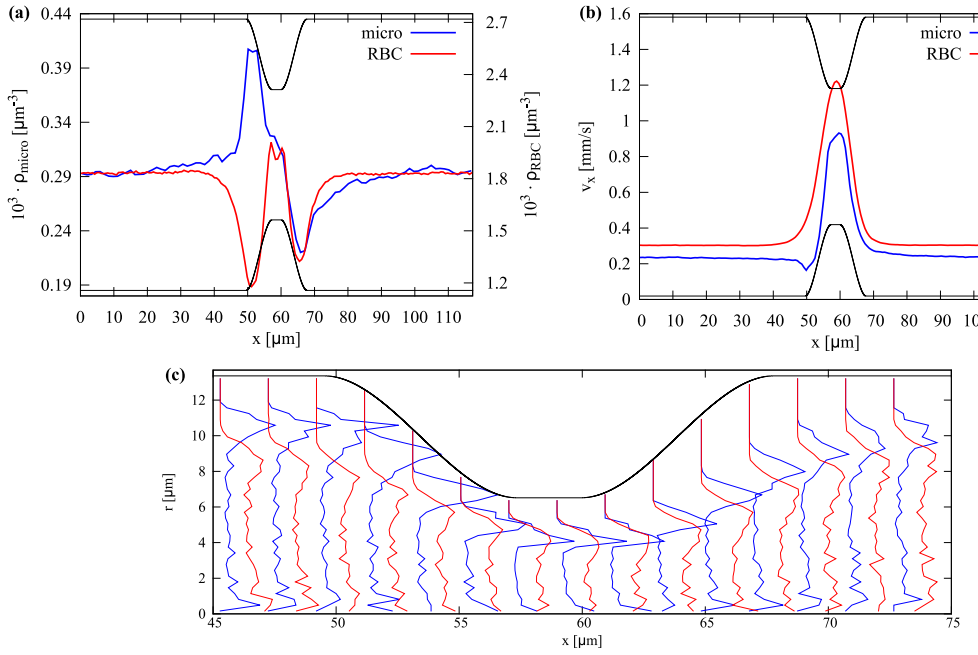

FIG. 4. (a) Concentration and (b) velocity as a function of axial position for the mixed suspension with Ht = 16.5% shown in Fig. 1(b). The RBCs (red curve) and the microparticles (blue curve) exhibit precisely opposite behavior in front of the constriction. While the RBCs decrease their concentration, the concentration of the microparticles significantly increases. (c) Concentration as a function of the radial position for various sites along the constriction. Inside the constriction the microparticles are located at same radial positions as the RBCs. The channel geometry is illustrated by the black line.

particles move towards the center, and the particle peak starts to overlap with the broad RBC profile [66]. Finally, inside the constricted part the microparticles and RBCs are located at similar radial positions, although the microparticles do retain a near-wall position in agreement with the planar situation investigated in Ref. [45] (although the authors did not observe the increase in concentration before the constriction). Regarding the RBCs themselves, we find that the cell-free layer thickness transiently increases at the exit of the constriction as in Refs. [38,45]. The pausing in front of the constriction also reflects itself in the microparticle velocity in Fig. 4(b). Whereas the RBC velocity monotonously increases ahead the constriction, the microparticle velocity exhibits a clear dip.

Thus, the effect of the same constriction is directly opposite for RBCs and marginated microparticles: while the RBCs are diluted, the concentration of the microparticles considerably increases in front of the constriction.

D. Influence of hematocrit

By increasing the number of RBCs in the system to 151, we investigate the influence of a higher hematocrit Ht = 23.7% as shown in Fig. 1(c). The axial concentration for Ht = 23.7% in Fig. 5(a) proves evidence that microparticle clustering also appears at higher Ht. Interestingly, despite the higher Ht in the main channel, the RBC concentration inside the constriction is nearly identical to the earlier case of Ht = 16.5%. This can be attributed to the discrete nature of the RBCs, which limits the amount of RBCs than can pass through the constriction per unit time as also observed in Ref. [38].

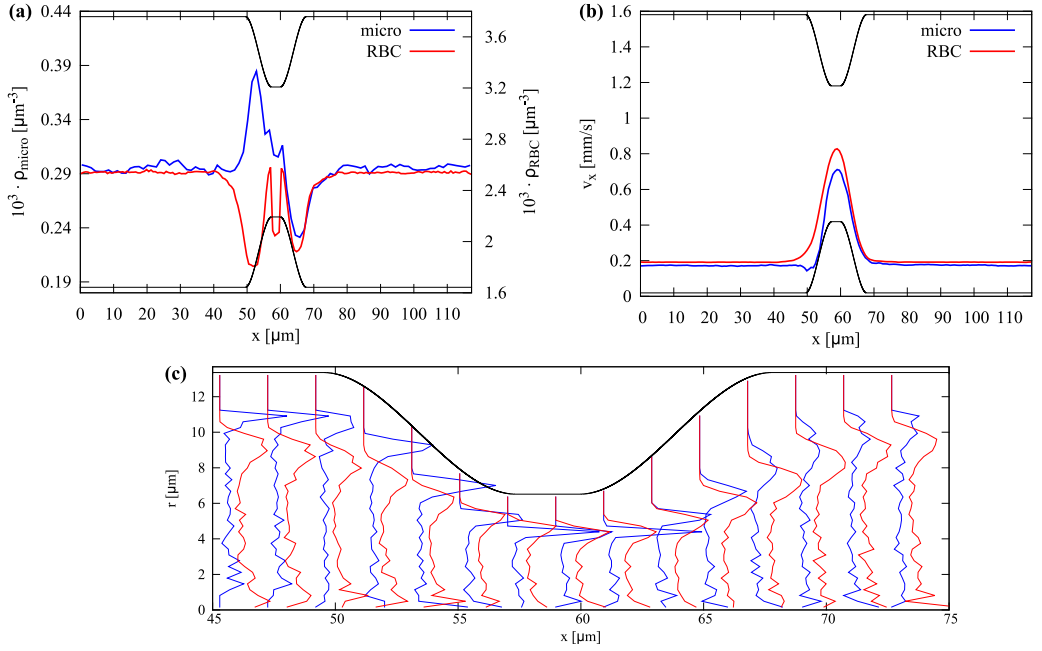

FIG. 5. (a) Concentration and (b) velocity as a function of axial position for a mixed suspension with hematocrit Ht = 23.7%. (c) Concentration as a function of the radial position for various sites along the constriction. The RBCs (red curve) exhibit the same behavior as for Ht = 16.5% in Fig. 4 except that the concentration inside the constriction is lower than in the main channel. The microparticles cluster in roughly the same amount ahead of the constriction. The channel geometry is illustrated by the black line.

In Fig. 5(c) the radial concentration profiles are shown for Ht = 23.7%. The dipping of microparticles into the RBC plug is present here in the same manner as for Ht = 16.5% in Fig. 4(c). While the velocity shown in Fig. 5(b) is in general lower due to the larger amount of cells, a dip in the microparticle velocity ahead the constriction is again observed.

The results for Ht = 23.7% suggest that an upper boundary for the extent of microparticle clustering exists. A possible explanation may be provided by the discrete motion of the RBCs through the constriction [38]. Due to the limited space inside the constriction, even for higher Ht the number of simultaneously passing RBCs is not strongly increased. As a consequence the probability for microparticles to find a gap and thus the clustering effect is nearly the same at both hematocrits.

E. Influence of constriction properties

To investigate the influence of the constriction properties we conduct one simulation with a longer constriction, a second with a narrower constriction, and a third with a longer (smoother) transition zone at Ht = 16.5%.

In the first simulation, the constricted part is four times longer than in Fig. 1(b). The observed axial concentration distribution is shown in Fig. 6(a). The microparticle concentration increases in front of the constriction in the same manner as for the short constriction (Fig. 4). Inside the constriction the microparticle concentration decreases slowly. We thus conclude that the clustering effect is independent of the length of the constriction.

The narrower constriction is chosen such that the ratio of the radii of the constricted part and the straight part equals 3/8 instead of 1/2 before. The increase in the microparticle concentration is significantly stronger [Fig. 6(b)] compared to Fig. 4. The explanation is straightforward: to pass the constriction a microparticle now has to migrate closer to the centerline. As explained before

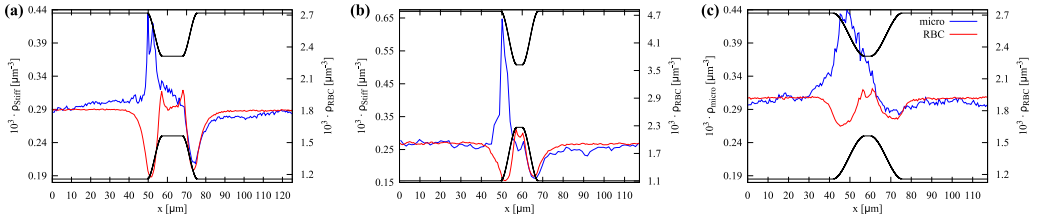

FIG. 6. Concentration as function of the axial position for the RBCs (red curve) and microparticles (blue curve) for (a) a four times longer constriction, (b) a narrower constriction with a radii ratio equaling 3/8, and (c) a twofold longer transition zone. The channel geometry is illustrated by the black line.

the collisions with the RBCs counteract this motion leading to a longer dwell time in front of the constriction.

Finally, we double the length of the transition zone between the main cylinder and the constricted part leading to a smoother transition. The observed concentration profile of the RBCs in Fig. 6(c) is similar to that in Fig. 4, except that the decrease ahead of and behind the constriction is less pronounced. This difference can be reproduced by the point particle method, which shows the same changes in the concentration profile (data not shown). Importantly, the amount of microparticle clustering is not influenced by the smoother transition.

These results lead us to suggest that the radius of the constriction is the important parameter that determines the amount of microparticle clustering: the narrower the constriction the stronger the clustering. However, microparticle clustering is independent of constriction length and transition zone.

F. Influence of particle shape and size

Finally, we investigate the behavior of stiff ellipsoids and larger spheres to study a possible influence of the particle shape and size at Ht = 16.5%. We use prolate ellipsoids with a long axis of 6.4 μm and a short axis of 3.2 μm (Fig. 7 inset) such that the short axis equals the diameter of the spheres used before. The larger spheres have a diameter of 4.9 μm. We find that ellipsoids and large spheres as well exhibit clustering in front of the constriction as shown in Fig. 7. Compared to the small spherical microparticles the increase in concentration ahead of the constriction is however less pronounced. The slightly reduced clustering can be explained by the increased size of the microparticles, which makes them dip more easily into the RBC plug and migrate towards the

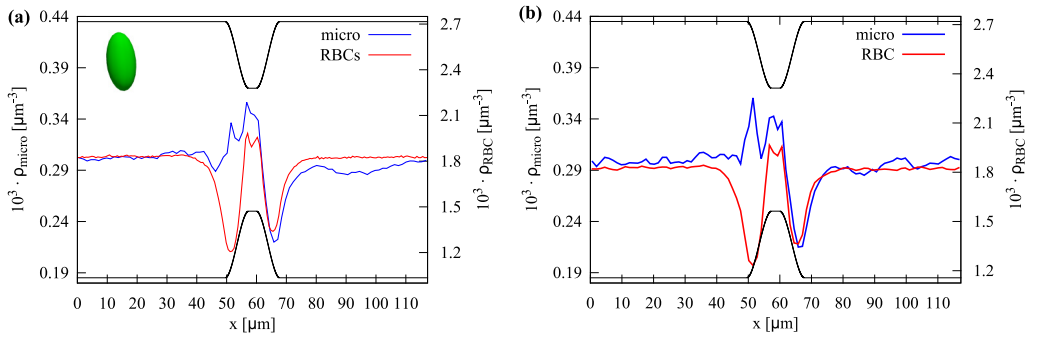

FIG. 7. (a) Center-of-mass density depending on the axial position for the RBCs (red curve) and the stiff ellipsoids (blue curve) in a RBC suspension flowing through a constriction. (b) The same data for large spheres with a diameter of 4.9 μm. Both microparticles cluster, but not in the same amount as the small spherical microparticles.

channel center. Nevertheless, the data suggest that clustering in front of constriction is a robust effect, which is qualitatively independent of the particle shape and size.

IV. CONCLUSION

We investigated the axial concentration of RBCs and microparticles in a mixed suspension flowing through a constricted cylindrical microchannel as a model system for a stenosis in the microcirculation. We found a pronounced peak in the microparticle concentration right in front of the constriction. This clustering of microparticles is explained by the marginated near-wall position, on which the microparticles arrive at the constriction and the corresponding more central position of the RBCs. As a consequence, microparticle passage through the constriction is severely hindered by the dense plug of RBCs occupying the channel center. Hence, the microparticles get stuck in front of the constriction until they find a suitable gap among the RBCs leading to a prolonged dwell time, which in the end causes the increased concentration. Interestingly, the RBCs themselves behave in a directly opposite manner, showing a dip in concentration before the constriction. Furthermore, we investigated the dependency on hematocrit, stenosis, particle size, and shape. The clustering effect is qualitatively robust.

Our discovery of microparticle clustering will be relevant for biochemically active particles such as drug delivery agents for which it will lead to higher activity in front of microstenoses occurring frequently in the microcirculation. Besides that, we expect that clustering of blood platelets by the mechanisms described in our work will increase the likelihood of microthrombus formation ahead of vessel stenoses [37,67–69].

ACKNOWLEDGMENTS

The authors thank the Gauss Centre for Supercomputing e.V. for providing computing time on the GCS Supercomputer SuperMUC at the Leibniz Supercomputing Centre. This work was supported by the Volkswagen Foundation.

[1] A. S. Popel and P. C. Johnson, Microcirculation and hemorheology, Annu. Rev. Fluid Mech. **37**, 43 (2005).
[2] C. Misbah and C. Wagner, Living fluids, C. R. Phys. **14**, 447 (2013).
[3] G. Gompper and D. A. Fedosov, Modeling microcirculatory blood flow: Current state and future perspectives, WIREs Syst. Biol. Med. **8**, 157 (2015).
[4] J. B. Freund, Numerical simulation of flowing blood cells, Annu. Rev. Fluid Mech. **46**, 67 (2014).
[5] G. W. Schmid-Schönbein, S. Usami, R. Skalak, and S. Chien, The interaction of leukocytes and erythrocytes in capillary and postcapillary vessels, Microvasc. Res. **19**, 45 (1980).
[6] E. C. Eckstein, A. W. Tilles, and F. J. Millero III, Conditions for the occurrence of large near-wall excesses of small particles during blood flow, Microvasc. Res. **36**, 31 (1988).
[7] A. Jain and L. L. Munn, Determinants of leukocyte margination in rectangular microchannels, PLoS ONE **4**, e7104 (2009).
[8] P. Charoenphol, R. B. Huang, and O. Eniola-Adefeso, Potential role of size and hemodynamics in the efficacy of vascular-targeted spherical drug carriers, Biomaterials **31**, 1392 (2010).
[9] T.-R. Lee, M. Choi, A. M. Kopacz, S.-H. Yun, W. K. Liu, and P. Decuzzi, On the near-wall accumulation of injectable particles in the microcirculation: Smaller is not better, Sci. Rep. **3**, 2079 (2013).
[10] H. Chen, J. I. Angerer, M. Napoleone, A. J. Reininger, S. W. Schneider, A. Wixforth, M. F. Schneider, and A. Alexander-Katz, Hematocrit and flow rate regulate the adhesion of platelets to Von Willebrand factor, Biomicrofluidics **7**, 064113 (2013).

[11] K. Namdee, A. J. Thompson, P. Charoenphol, and O. Eniola-Adefeso, Margination propensity of vascular-targeted spheres from blood flow in a microfluidic model of human microvessels, Langmuir **29**, 2530 (2013).
[12] G. Wang, W. Mao, R. Byler, K. Patel, C. Henegar, A. Alexeev, and T. Sulchek, Stiffness dependent separation of cells in a microfluidic device, PLoS ONE **8**, e75901 (2013).
[13] S. Fitzgibbon, A. P. Spann, Q. M. Qi, and E. S. G. Shaqfeh, In vitro measurement of particle margination in the microchannel flow: Effect of varying hematocrit, Biophys. J. **108**, 2601 (2015).
[14] R. D'Apolito, G. Tomaiuolo, F. Taraballi, S. Minardi, D. Kirui, X. Liu, A. Cevenini, R. Palomba, M. Ferrari, F. Salvatore, E. Tasciotti, and S. Guido, Red blood cells affect the margination of microparticles in synthetic microcapillaries and intravital microcirculation as a function of their size and shape, J. Control. Release **217**, 263 (2015).
[15] R. D'Apolito, F. Taraballi, S. Minardi, X. Liu, S. Caserta, A. Cevenini, E. Tasciotti, G. Tomaiuolo, and S. Guido, Microfluidic interactions between red blood cells and drug carriers by image analysis techniques, Med. Eng. Phys. **38**, 17 (2015).
[16] C. Migliorini, Y. H. Qian, H. Chen, E. B. Brown, R. K. Jain, and L. L. Munn, Red blood cells augment leukocyte rolling in a virtual blood vessel, Biophys. J. **83**, 1834 (2002).
[17] J. B. Freund, Leukocyte margination in a model microvessel, Phys. Fluids **19**, 023301 (2007).
[18] L. Crowl and A. L. Fogelson, Analysis of mechanisms for platelet near-wall excess under arterial blood flow conditions, J. Fluid Mech. **676**, 348 (2011).
[19] A. Kumar and M. D. Graham, Segregation by membrane rigidity in flowing binary suspensions of elastic capsules, Phys. Rev. E **84**, 066316 (2011).
[20] A. A. Tokarev, A. A. Butylin, E. A. Ermakova, E. E. Shnol, G. P. Panasenko, and F. I. Ataullakhanov, Finite platelet size could be responsible for platelet margination effect, Biophys. J. **101**, 1835 (2011).
[21] H. Zhao and E. S. G. Shaqfeh, Shear-induced platelet margination in a microchannel, Phys. Rev. E **83**, 061924 (2011).
[22] H. Zhao, E. S. G. Shaqfeh, and V. Narsimhan, Shear-induced particle migration and margination in a cellular suspension, Phys. Fluids **24**, 011902 (2012).
[23] A. Kumar and M. D. Graham, Mechanism of Margination in Confined Flows of Blood and Other Multicomponent Suspensions, Phys. Rev. Lett. **109**, 108102 (2012).
[24] D. A. Fedosov, J. Fornleitner, and G. Gompper, Margination of White Blood Cells in Microcapillary Flow, Phys. Rev. Lett. **108**, 028104 (2012).
[25] J. B. Freund and B. Shapiro, Transport of particles by magnetic forces and cellular blood flow in a model microvessel, Phys. Fluids **24**, 051904 (2012).
[26] D. A. Reasor, M. Mehrabadi, D. N. Ku, and C. K. Aidun, Determination of critical parameters in platelet margination, Ann. Biomed. Eng. **41**, 238 (2013).
[27] A. Kumar, R. G. Henríquez Rivera, and M. D Graham, Flow-induced segregation in confined multicomponent suspensions: Effects of particle size and rigidity, J. Fluid Mech. **738**, 423 (2014).
[28] D. A. Fedosov and G. Gompper, White blood cell margination in microcirculation, Soft Matter **10**, 2961 (2014).
[29] K. Müller, D. A. Fedosov, and G. Gompper, Margination of micro- and nano-particles in blood flow and its effect on drug delivery, Sci. Rep. **4**, 4871 (2014).
[30] K. Vahidkhah, S. L. Diamond, and P. Bagchi, Platelet dynamics in three-dimensional simulation of whole blood, Biophys. J. **106**, 2529 (2014).
[31] K. Vahidkhah and P. Bagchi, Microparticle shape effects on margination, near-wall dynamics and adhesion in a three-dimensional simulation of red blood cell suspension, Soft Matter **11**, 2097 (2015).
[32] R. G. Henríquez Rivera, K. Sinha, and M. D. Graham, Margination Regimes and Drainage Transition in Confined Multicomponent Suspensions, Phys. Rev. Lett. **114**, 188101 (2015).
[33] K. Müller, D. A. Fedosov, and G. Gompper, Understanding particle margination in blood flow: A step toward optimized drug delivery systems, Med. Eng. Phys. **38**, 2 (2016).
[34] S. Gekle, Strongly accelerated margination of active particles in blood flow, Biophys. J. **110**, 514 (2016).
[35] T. Krüger, Effect of tube diameter and capillary number on platelet margination and near-wall dynamics, Rheol. Acta **55**, 511 (2016).

[36] M. Mehrabadi, D. N. Ku, and C. K. Aidun, Effects of shear rate, confinement, and particle parameters on margination in blood flow, Phys. Rev. E **93**, 023109 (2016).
[37] A. P. Spann, J. E. Campbell, S. R. Fitzgibbon, A. Rodriguez, A. P. Cap, L. H. Blackbourne, and E. S. G. Shaqfeh, The effect of hematocrit on platelet adhesion: Experiments and simulations, Biophys. J. **111**, 577 (2016).
[38] K. Vahidkhah, P. Balogh, and P. Bagchi, Flow of red blood cells in stenosed microvessels, Sci. Rep. **6**, 28194 (2016).
[39] L. Mountrakis, E. Lorenz, and A. G. Hoekstra, Where do the platelets go? A simulation study of fully resolved blood flow through aneurysmal vessels, Interface Focus **3**, 20120089 (2013).
[40] R. Zhao, J. N. Marhefka, F. Shu, S. J. Hund, M. V. Kameneva, and J. F. Antaki, Micro-flow visualization of red blood cell-enhanced platelet concentration at sudden expansion, Ann. Biomed. Eng. **36**, 1130 (2008).
[41] M. Faivre, M. Abkarian, K. Bickraj, and H. A. Stone, Geometrical focusing of cells in a microfluidic device: An approach to separate blood plasma, Biorheology **43**, 147 (2006).
[42] H. Fujiwara, T. Ishikawa, R. Lima, N. Matsuki, Y. Imai, H. Kaji, M. Nishizawa, and T. Yamaguchi, Red blood cell motions in high-hematocrit blood flowing through a stenosed microchannel, J. Biomech. **42**, 838 (2009).
[43] W. Wang, T. G. Diacovo, J. Chen, J. B. Freund, and M. R. King, Simulation of platelet, thrombus and erythrocyte hydrodynamic interactions in a 3D arteriole with in vivo comparison, PLoS ONE **8**, e76949 (2013).
[44] T. Skorczewski, L. C. Erickson, and A. L. Fogelson, Platelet motion near a vessel wall or thrombus surface in two-dimensional whole blood simulations, Biophys. J. **104**, 1764 (2013).
[45] A. Yazdani and G. E. Karniadakis, Sub-cellular modeling of platelet transport in blood flow through microchannels with constriction, Soft Matter **12**, 4339 (2016).
[46] H. J. Limbach, A. Arnold, B. A. Mann, and C. Holm, ESPResSo: An extensible simulation package for research on soft matter systems, Comput. Phys. Commun. **174**, 704 (2006).
[47] D. Roehm and A. Arnold, Lattice Boltzmann simulations on GPUs with ESPResSo, Eur. Phys. J. Special Topics **210**, 89 (2012).
[48] A. Arnold, O. Lenz, S. Kesselheim, R. Weeber, F. Fahrenberger, D. Roehm, P. Košovan, and C. Holm, Espresso 3.1: Molecular dynamics software for coarse-grained models, in *Meshfree Methods for Partial Differential Equations VI*, edited by M. Griebel and M. A. Schweitzer (Springer, Berlin, 2013), pp. 1–23.
[49] C. S. Peskin, The immersed boundary method, Acta Numerica **11**, 479 (2002).
[50] R. Mittal and G. Iaccarino, Immersed boundary methods, Annu. Rev. Fluid Mech. **37**, 239 (2005).
[51] S. Succi, *The Lattice Boltzmann Equation: For Fluid Dynamics and Beyond* (Oxford University Press, Oxford, 2001).
[52] B. Dünweg and A. J. C. Ladd, in *Advanced Computer Simulation Approaches for Soft Matter Sciences III*, edited by C. Holm and K. Kremer (Springer, Berlin, 2008), p. 89.
[53] C. K. Aidun and J. R. Clausen, Lattice-Boltzmann method for complex flows, Annu. Rev. Fluid Mech. **42**, 439 (2010).
[54] D. Barthès-Biesel, Modeling the motion of capsules in flow, Curr. Opin. Colloid Interface Sci. **16**, 3 (2011).
[55] J. B. Freund, The flow of red blood cells through a narrow spleen-like slit, Phys. Fluids **25**, 110807 (2013).
[56] A. Farutin, T. Biben, and C. Misbah, 3D numerical simulations of vesicle and inextensible capsule dynamics, J. Comput. Phys. **275**, 539 (2014).
[57] A. Daddi-Moussa-Ider, A. Guckenberger, and S. Gekle, Long-lived anomalous thermal diffusion induced by elastic cell membranes on nearby particles, Phys. Rev. E **93**, 012612 (2016).
[58] A. Guckenberger, M. P. Schraml, P. G. Chen, M. Leonetti, and S. Gekle, On the bending algorithms for soft objects in flows, Comput. Phys. Commun. **207**, 1 (2016).
[59] See Supplemental Material at http://link.aps.org/supplemental/10.1103/PhysRevFluids.2.013102 for the influence of the channel length and further velocity and axial concentration profiles for the simulations with different stenosis properties, and with ellipsoidal and larger particles. The video illustrates the main system shown in Fig. 1(b).

[60] G. Coupier, B. Kaoui, T. Podgorski, and C. Misbah, Noninertial lateral migration of vesicles in bounded Poiseuille flow, Phys. Fluids **20**, 111702 (2008).
[61] T. M. Geislinger, B. Eggart, S. Braunmüller, L. Schmid, and T. Franke, Separation of blood cells using hydrodynamic lift, Appl. Phys. Lett. **100**, 183701 (2012).
[62] X. Grandchamp, G. Coupier, A. Srivastav, C. Minetti, and T. Podgorski, Lift and Down-Gradient Shear-Induced Diffusion in Red Blood Cell Suspensions, Phys. Rev. Lett. **110**, 108101 (2013).
[63] D. A. Fedosov, B. Caswell, A. S. Popel, and G. E. Karniadakis, Blood flow and cell-free layer in microvessels, Microcirculation **17**, 615 (2010).
[64] J. B. Freund and M. M. Orescanin, Cellular flow in a small blood vessel, J. Fluid. Mech. **671**, 466 (2011).
[65] D. Katanov, G. Gompper, and D. A. Fedosov, Microvascular blood flow resistance: Role of red blood cell migration and dispersion, Microvasc. Res. **99**, 57 (2015).
[66] Note that due to the azimuthal and temporal averaging contained in the concentration profiles this does not imply physical overlap of individual particles.
[67] W. S. Nesbitt, E. Westein, F. J. Tovar-Lopez, E. Tolouei, A. Mitchell, J. Fu, J. Carberry, A. Fouras, and S. P. Jackson, A shear gradient–dependent platelet aggregation mechanism drives thrombus formation, Nature Med. **15**, 665 (2009).
[68] F. J. Tovar-Lopez, G. Rosengarten, M. Nasabi, V. Sivan, K. Khoshmanesh, S. P. Jackson, A. Mitchell, and W. S. Nesbitt, An investigation on platelet transport during thrombus formation at micro-scale stenosis, PLoS ONE **8**, e74123 (2013).
[69] A. L. Folgelson and K. B. Neeves, Fluid mechanics of blood clot formation, Annu. Rev. Fluid Mech. **47**, 377 (2015).